

Ultrafast carbothermal shock synthesis of transition metal phosphides in air for highly efficient hydrogen evolution reaction

Tingting Liu , Ruting Lin , Yuyu Liua Chen Chen , Qiufeng Huang ,  
Yuzhi Sun , Shengyun Huang , Ibrahim Saana Amiinu ,  
Zonghua Pu

PII: S1001-8417(25)00497-8  
DOI: <https://doi.org/10.1016/j.cclet.2025.111312>  
Reference: CCLET 111312



To appear in: *Chinese Chemical Letters*

Please cite this article as: Tingting Liu , Ruting Lin , Yuyu Liua Chen Chen , Qiufeng Huang ,  
Yuzhi Sun , Shengyun Huang , Ibrahim Saana Amiinu , Zonghua Pu , Ultrafast carbothermal shock  
synthesis of transition metal phosphides in air for highly efficient hydrogen evolution reaction, *Chinese  
Chemical Letters* (2025), doi: <https://doi.org/10.1016/j.cclet.2025.111312>

This is a PDF file of an article that has undergone enhancements after acceptance, such as the addition of a cover page and metadata, and formatting for readability, but it is not yet the definitive version of record. This version will undergo additional copyediting, typesetting and review before it is published in its final form, but we are providing this version to give early visibility of the article. Please note that, during the production process, errors may be discovered which could affect the content, and all legal disclaimers that apply to the journal pertain.

© 2025 Published by Elsevier B.V. on behalf of Chinese Chemical Society and Institute of Materia Medica, Chinese Academy of Medical Sciences.

# Ultrafast carbothermal shock synthesis of transition metal phosphides in air for highly efficient hydrogen evolution reaction

Tingting Liu,<sup>a,1</sup> Ruting Lin,<sup>a,1</sup> Yuyu Liu,<sup>a</sup> Chen Chen,<sup>a</sup> Qiufeng Huang,<sup>a</sup> Yuzhi Sun,<sup>b</sup> Shengyun Huang,<sup>b,\*</sup> Ibrahim Saana Amiinu,<sup>c</sup> Zonghua Pu<sup>a,\*\*</sup>

<sup>a</sup> College of Chemistry & Materials Science, Fujian Normal University, Fuzhou 350117, China

<sup>b</sup> Ganjiang Innovation Academy, Key Laboratory of Rare Earths, Chinese Academy of Sciences, Ganzhou 341000, China

<sup>c</sup> Department of Chemical Sciences, University of Limerick, Limerick, V94 T9PX, Ireland

## ARTICLE INFO

### Article history:

Received

Received in revised form

Accepted

Available online

### Keywords:

Ultrafast synthesis

Joule heating

Metal phosphides

Hydrogen evolution reaction

Electrocatalysis

## ABSTRACT

Transition metal phosphides (TMPs) are a promising class of functional nanomaterials with significant potential for energy-related applications. However, a universal synthesis method that is both efficient and scalable remains a challenge. This study introduces an ultrafast carbothermal shock (UCS) technique as efficient method for synthesizing various TMPs, including Rh<sub>2</sub>P, Ir<sub>2</sub>P, Pd<sub>5</sub>P<sub>2</sub>, RuP and PtP<sub>2</sub>, in just 15 s under ambient air conditions. Notably, the as synthesized Rh<sub>2</sub>P exhibits remarkable hydrogen evolution reaction (HER) performance with low overpotentials of 13 and 70 mV to reach current densities of 10 and 100 mA/cm<sup>2</sup>, respectively, coupled with excellent operational stability for over 20 h. This technique not only provides a universal platform for producing various metal phosphides, but also holds significant promise for advancing their applications in energy conversion and storage devices, catalysis, and biosensors.

Reconciling the development of a sustainable, global-scale energy system concurrently with the preservation of the environment stands as one of the most critical challenges facing humanity. To date, over 80% of the energy resources supporting modern society stems from traditional fossil fuels [1-3]. Therefore, leveraging renewable energy sources, including solar, wind, marine, and hydroelectric power for electrochemical energy conversion and storage represents a promising approach to achieving energy sustainability [4-13]. In this context, clean energy storage and conversion technologies, such as hydrogen production *via* water electrolysis, various rechargeable battery systems, and fuel cells have attracted significant research interest [14-20]. Hydrogen and oxygen evolution reactions (HER and OER) are crucial electrokinetic processes for hydrogen production. Likewise, efficient oxygen reduction and evolution reactions (ORR and OER) are essential for the renewable energy sector, especially in the development of fuel cells and rechargeable batteries [21,22]. Thus, the development of catalytic system with high stability and enhanced performance for HER, OER and ORR are vital for the aforementioned energy storage and conversion systems.

In the past ten years, transition-metal phosphides (TMPs) have received considerable attention for their applications in electrocatalysis due to their outstanding physicochemical properties, including good conductivity and high catalytic activities [23,24], [25-32]. However, achieving metal phosphides with stable crystal structure requires prolonged high-temperature pyrolysis ( $\geq 2$ h) under the inert atmosphere, which is not only time-consuming and energy-intensive but also escalates production costs. Furthermore, the extended high-temperature calcination process generates substantial CO<sub>2</sub> emissions. These factors contribute to increased production costs. Additionally, the toxic phosphine gas (PH<sub>3</sub>) generated during traditional calcination can cause severe air pollution. Similarly, the dissolution-thermal method produces phosphorus-containing wastewater and organic solvent emissions, imposing supplementary economic and environmental burdens. More importantly, traditional methods often result in large particle sizes as well as agglomeration, ultimately resulting in a decline in electrochemical performance. Therefore, it is highly desirable to explore rapid synthetic approaches that enable the production of nano-sized TMP particles with enhanced surface area at lower pyrolysis temperatures and ambient air conditions. Fortunately, ultrafast carbothermal shock (UCS) synthesis allows for rapid flash heating and cooling, with ramp rates reaching up to 10<sup>5</sup> K/s. This instantaneous temperature fluctuation allows reactions to complete within few seconds [33-36]. The total energy consumption is significantly reduced. On the other hand, UCS holds significant potential for continuous production, leading to lower long-term operating costs and reduced per-unit production costs as scale increases. Additionally, the low energy consumption of UCS effectively decreases carbon emissions, aligning with the principles of green manufacturing. More importantly, the optimized second-level calcination time effectively mitigates sintering and agglomeration of active components that could result from prolonged heat treatment, thereby ensuring the rapid and uniform dispersion of active atoms. This enhancement facilitates precise control over the particle size and structure of the synthesized materials.

Herein, we have successfully demonstrated an ultrafast ( $\leq 15$ s), energy-saving synthesis of a series of TMPs, including Rh<sub>2</sub>P, Ir<sub>2</sub>P, Pd<sub>5</sub>P<sub>2</sub>, RuP, and PtP<sub>2</sub>, using UCS under ambient air atmosphere. Characterization results indicate that these TMPs comprise of

\* Corresponding authors.

E-mail addresses: [shyhuang@gia.cas.cn](mailto:shyhuang@gia.cas.cn) (S. Huang), [zonghua.pu@fjnu.edu.cn](mailto:zonghua.pu@fjnu.edu.cn) (Z. Pu).

<sup>1</sup> This authors contributed equally to this work.

ultrasmall nanoparticles with controllable sizes and well-defined crystalline structures, with enhanced HER activity and stability. For example, the as obtained Rh<sub>2</sub>P exhibits platinum-like HER activity with overpotentials of 13 and 70 mV at a current density of 10 and 100 mA/cm<sup>2</sup> in 0.5 mol/L H<sub>2</sub>SO<sub>4</sub>, respectively. Such high HER activities not only surpass most reported electrocatalysts based on precious-metal phosphides, but also compared favorably to commercial Pt/C materials. Therefore, this study presents a pioneering approach to fabricating TMPs in seconds by UCS under ambient air conditions with enhanced HER performance.

The UCS synthesis process for these TMPs nanoparticles is schematically illustrated in Fig. 1a. Initially, a homogeneous mixture of metal salts and NH<sub>4</sub>H<sub>2</sub>PO<sub>2</sub> was prepared. Subsequently, the obtained precursor mixture was subjected to UCS under air atmosphere. Following cooling, the byproduct was extensively rinsed with deionized water to obtain the final sample. Notably, the UCS strategy enables the synthesis of various TMPs, including Rh<sub>2</sub>P, Ir<sub>2</sub>P, Pd<sub>5</sub>P<sub>2</sub>, RuP, and PtP<sub>2</sub> (Fig. 1b). For comparison, Rh<sub>2</sub>P-T was also prepared *via* the calcination process in a tube furnace. As shown in Fig. S1a (Supporting information), the XRD pattern confirming the Rh<sub>2</sub>P-T has been successfully obtained. Furthermore, TEM images show that Rh<sub>2</sub>P-T exhibits a bulk morphology (Figs. S1b, c and S2 in Supporting information).

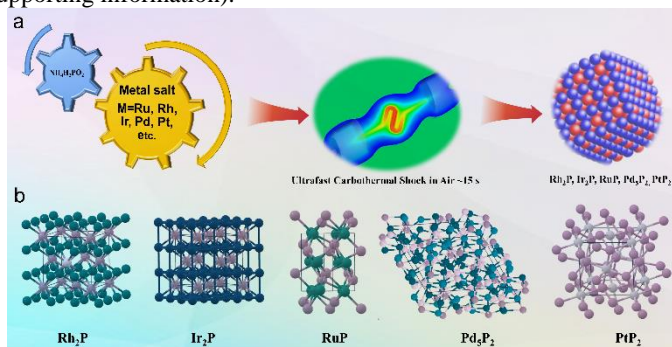


**Fig. 1.** (a) Schematic illustration of the synthesis process of TMPs by UCS. (b) The crystal structures of Rh<sub>2</sub>P, Ir<sub>2</sub>P, Pd<sub>5</sub>P<sub>2</sub>, RuP, and PtP<sub>2</sub>. Purple and black-blue balls denote phosphorus and metal elements.

Powder X-ray diffraction (XRD) was used to investigate the crystallographic structure of Rh<sub>2</sub>P, Ir<sub>2</sub>P, Pd<sub>5</sub>P<sub>2</sub>, RuP, and PtP<sub>2</sub>. As displayed in Figs. 2a, d, g, j and m, the diffraction patterns of Rh<sub>2</sub>P, Ir<sub>2</sub>P, Pd<sub>5</sub>P<sub>2</sub>, RuP, and PtP<sub>2</sub> match well with their standard PDF cards [37, 38]. The structural features of Rh<sub>2</sub>P, Ir<sub>2</sub>P, Pd<sub>5</sub>P<sub>2</sub>, RuP, and PtP<sub>2</sub> are revealed by TEM (Figs. 2b, c, e, f, h, i, k, l, n and o). The TEM images in Figs. 2b and h indicate that Rh<sub>2</sub>P and RuP are composed of small nanocrystals. The Ir<sub>2</sub>P shows a nanosphere morphology with particle size ranges from 8 nm to 25 nm (Fig. 2e and Fig. S3 in Supporting information), while both Pd<sub>5</sub>P<sub>2</sub> and PtP<sub>2</sub> possess a typical nanoparticles structure with particle size of ~2 and 20 nm, respectively (Figs. 2k and n, Fig. S3). Additionally, the high-resolution TEM (HRTEM) images reveal the lattice fringe spacing of Rh<sub>2</sub>P, Ir<sub>2</sub>P, RuP, Pd<sub>5</sub>P<sub>2</sub> and PtP<sub>2</sub> to be 0.195, 0.278, 0.306, 0.228 and 0.285 nm, corresponding to cubic Rh<sub>2</sub>P (220), cubic Ir<sub>2</sub>P (200), orthorhombic RuP (200), monoclinic Pd<sub>5</sub>P<sub>2</sub> (113) and cubic PtP<sub>2</sub> (200) crystal planes (Figs. 2c, f, i, l and o), respectively.

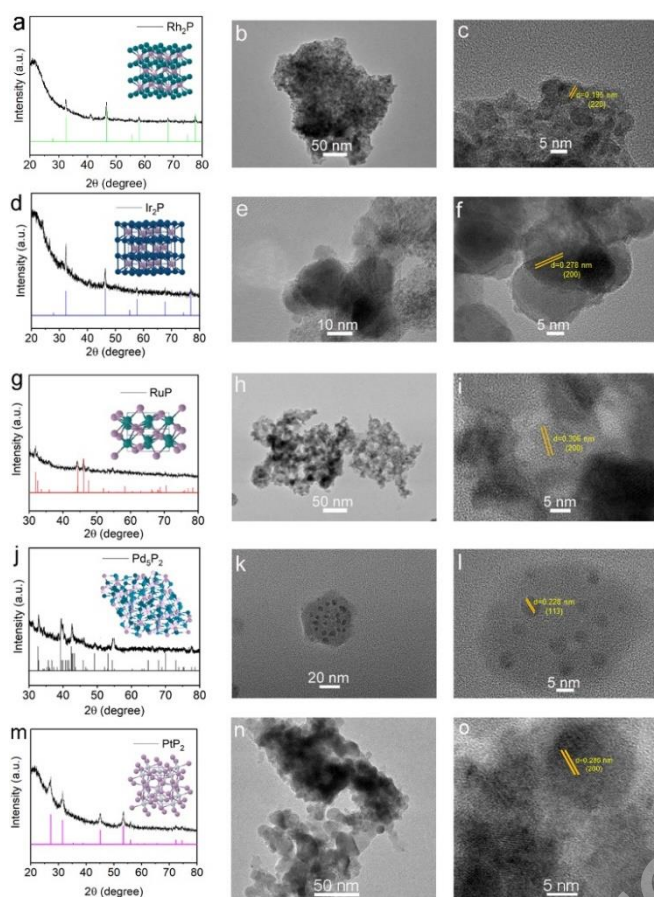


**Fig. 2.** (a) The XRD patterns for (a)  $\text{Rh}_2\text{P}$ , (d)  $\text{Ir}_2\text{P}$ , (g)  $\text{RuP}$ , (j)  $\text{Pd}_3\text{P}_2$  and (m)  $\text{PtP}_2$ . TEM and HRTEM images of (b, c)  $\text{Rh}_2\text{P}$ , (e, f)  $\text{Ir}_2\text{P}$ , (h, i)  $\text{RuP}$ , (k, l)  $\text{Pd}_3\text{P}_2$  and (m, n)  $\text{PtP}_2$ .

The energy dispersive X-ray (EDX) spectrum (Fig. S4 in Supporting information) confirms the presence of Rh and P in the  $\text{Rh}_2\text{P}$  nanoparticle, with an atomic ratio of Rh and P approaching 2:1. Furthermore, the HAADF-STEM and energy-dispersive X-ray spectroscopy (EDS) elemental mapping demonstrate homogeneous distribution of both Rh and P elements within the  $\text{Rh}_2\text{P}$  nanoparticle (Figs. 3a-d). These results demonstrate that the UCS process is energy-efficient and time-saving for fabricating a series of uniformly dispersed TMPs under an air atmosphere.

XPS was employed to further examine the elemental composition and surface chemical state of  $\text{Rh}_2\text{P}$ . The results indicate that the surface of  $\text{Rh}_2\text{P}$  is predominantly composed of C, O, Rh and P (Fig. S5 in Supporting information). The presence of elemental C and O can be assigned to the absorption of  $\text{CO}_2$ ,  $\text{H}_2\text{O}$ ,  $\text{O}_2$ , or slight surface oxidation of  $\text{Rh}_2\text{P}$  potentially caused by exposure to air. The XPS spectrum of the Rh3d region exhibits two peaks at binding energies (BE) of 312.6 and 307.8 eV, corresponding to the Rh 3d<sub>3/2</sub> and Rh 3d<sub>5/2</sub> states of  $\text{Rh}_2\text{P}$  (Fig. 3e), respectively. In addition, the P 2p spectrum displays three distinct subpeaks at 133.9, 131.2 and 130.1 eV (Fig. 3f). The peaks observed at 131.2 and 130.1 eV can be attributed to the Rh-P bond, whereas the peak at 133.9 eV is indicative of oxidized phosphorus species. Notably, the Rh 3d<sub>5/2</sub> peak is blue-shifted by 0.5 eV relative to the metal Rh (307.3 eV) [39], while the P 2p<sub>3/2</sub> peak is red-shifted compared to elemental P (130.2 eV) [40]. These observations indicate the presence of a partial positive charge ( $\delta^+$ ) on Rh and a partial negative charge ( $\delta^-$ ) on P in  $\text{Rh}_2\text{P}$ , suggesting a weak electron transfer from Rh to P. The positively charged Rh atom serve as the hydride-acceptor center, while the negatively charged P atom functions as the proton-acceptor center. This dual functionality modulates the attachment and detachment of hydrogen atoms at the active sites during the subsequent HER process.

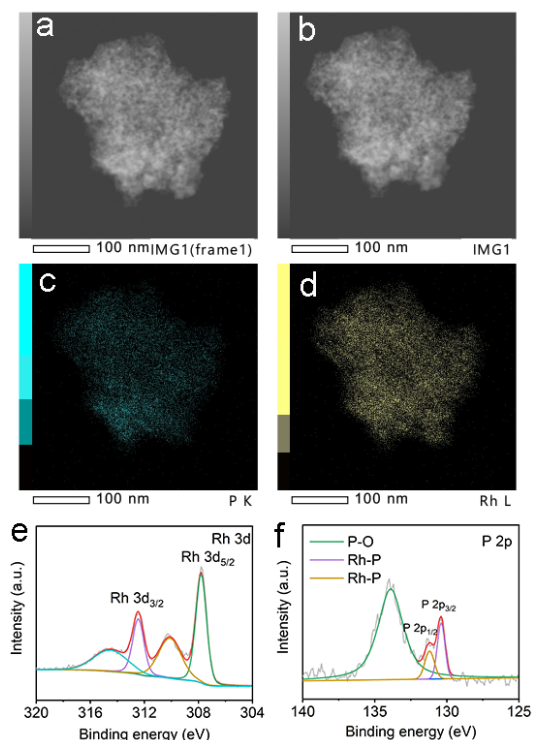


**Fig. 3.** (a-d) STEM images and corresponding EDS elemental mapping of Rh and P of Rh<sub>2</sub>P. (e) Rh 3d and (f) P 2p XPS spectra of Rh<sub>2</sub>P.

The HER activity of the obtained samples (Rh<sub>2</sub>P, PtP<sub>2</sub>, Ir<sub>2</sub>P, RuP and Pd<sub>5</sub>P<sub>2</sub>) were examined in 0.5 mol/L H<sub>2</sub>SO<sub>4</sub> electrolytes, with all potentials calibrated using an RHE as the reference scale. Before conducting the HER tests, the obtained samples were activated by performing a series of linear sweep voltammetry (LSV) scans ranging from 0 to -0.5 V vs. Ag/AgCl. Fig. 4a illustrates the *iR*-corrected (the internal resistance determined through EIS analysis in Fig. S6 in Supporting information) HER polarization curves of Rh<sub>2</sub>P, PtP<sub>2</sub>, Ir<sub>2</sub>P, RuP and Pd<sub>5</sub>P<sub>2</sub>. All the samples (Rh<sub>2</sub>P, PtP<sub>2</sub>, Ir<sub>2</sub>P, RuP and Pd<sub>5</sub>P<sub>2</sub>) obtained *via* UCS exhibits good HER catalytic activities with an onset potential close to 0 mV. Specifically, the overpotentials needed for Rh<sub>2</sub>P, PtP<sub>2</sub>, Ir<sub>2</sub>P, RuP and Pd<sub>5</sub>P<sub>2</sub> to achieve a cathodic current density of 10 mA/cm<sup>2</sup> are 13, 20, 37, 30 and 84 mV (Fig. 4b), respectively. More importantly, the catalytic activity of Rh<sub>2</sub>P, PtP<sub>2</sub>, Ir<sub>2</sub>P, RuP and Pd<sub>5</sub>P<sub>2</sub> is comparable to that of recently reported Rh/Pt/Ir/Ru/Pd-based TMPs synthesized by traditional methods, such as Rh<sub>2</sub>P obtained by solution-phase reaction (14 mV@10 mA/cm<sup>2</sup>) [41], PtP<sub>2</sub>@NPC synthesized by high-temperature pyrolysis of mixtures of PtCl<sub>4</sub> with phytic acid under an ammonia atmosphere (320 mV@10 mA/cm<sup>2</sup>) [42], Ir<sub>2</sub>P-decorated Ru<sub>2</sub>P hollow nanotubes *via* an anion/cation-exchange strategy (23.2 mV@10 mA/cm<sup>2</sup>) [43], RuP<sub>2</sub>@NPC obtained by thermal treatment (38 mV@10 mA/cm<sup>2</sup>) [44], Pd<sub>5</sub>P<sub>2</sub>@NPGC synthesized by traditional pyrolysis (104 mV@10 mA/cm<sup>2</sup>) [45]. This observation suggests the superiority of UCS over conventional methods in preparing TMPs. Tafel slope is another critical parameter for assessing the HER activity of electrocatalysts. The Tafel slopes obtained from the linear region of the Tafel plots for Rh<sub>2</sub>P, PtP<sub>2</sub>, Ir<sub>2</sub>P, RuP and Pd<sub>5</sub>P<sub>2</sub> are 30, 49, 51, 70 and 110 mV/dec (Fig. 4c), respectively. Similarly, these Tafel values are comparable to those reported for Pt-group TMPs synthesized using conventional ways [41-45]. Furthermore, taking Rh<sub>2</sub>P as the research object, based on its Tafel value, it can be inferred that the hydrogen generation process of Rh<sub>2</sub>P in acidic solutions likely follows the Volmer-Tafel mechanism, and the rate-determining step (RDS) is governed by the Tafel step: 2M-H<sub>ad</sub> → H<sub>2</sub> + 2M, where M denotes the active site and H<sub>ad</sub> represents the adsorbed hydrogen intermediate [46,47]. To the best of our knowledge, the high HER activity of these samples compares favorably with that of most TMPs synthesized by traditional methods (such as pyrolysis at high temperature in inert atmosphere or solution synthesis in organic solvents) reported in acidic electrolytes (Fig. 4d and Table S2 in Supporting information).

Based on the superior HER activity demonstrated by Rh<sub>2</sub>P, we conducted an in-depth investigation into its long-term stability. Fig. 4e presents the polarization curves obtained before and after 1000 cyclic voltammetry (CV) cycles at 5 mV/s. It is worth noting that the LSV curves of Rh<sub>2</sub>P exhibited minimal degradation even after undergoing 1000 CV potential cycles. Furthermore, the long-term stability of the Rh<sub>2</sub>P electrocatalyst is evaluated through continuous electrolysis at a fixed overpotential of ~20 mV without *iR* correction. As shown in Fig. 4f, the current density of Rh<sub>2</sub>P demonstrates negligible degradation under acidic conditions over 20 h electrolysis period, highlighting the exceptional durability of the synthesized Rh<sub>2</sub>P. Additionally, the XRD analysis of both the fresh and post-HER Rh<sub>2</sub>P materials (Fig. S7 in Supporting information) confirms the similarity in their crystal structures. Furthermore, inductively coupled plasma atomic emission spectroscopy (ICP-AES) analysis revealed that rhodium exhibited minimal leaching (6%) in the electrolyte during prolonged stability testing. This limited leaching may be attributed to the partial desorption of powder electrocatalysts from the electrode surfaces due to vigorous gas evolution during the HER [48]. These results offering robust evidence for the retention of the Rh<sub>2</sub>P composition and its remarkable durability under acidic media during HER.

More significantly, Rh<sub>2</sub>P exhibits excellent HER performance under both alkaline (1.0 mol/L KOH) and neutral (1.0 mol/L PBS) conditions, requiring overpotentials of 70 and 97 mV, respectively, to achieve a current density of 10 mA/cm<sup>2</sup> (Fig. S8 in Supporting information). Additionally, it exhibits stable performance with operation durations of 8 h in neutral electrolytes (1.0 mol/L PBS) and 11



h in alkaline electrolytes (1.0 mol/L KOH) (Fig. S9 in Supporting information). Therefore, these comprehensive analyses demonstrate that Rh<sub>2</sub>P is an excellent and durable catalyst material for HER in a wide pH range.

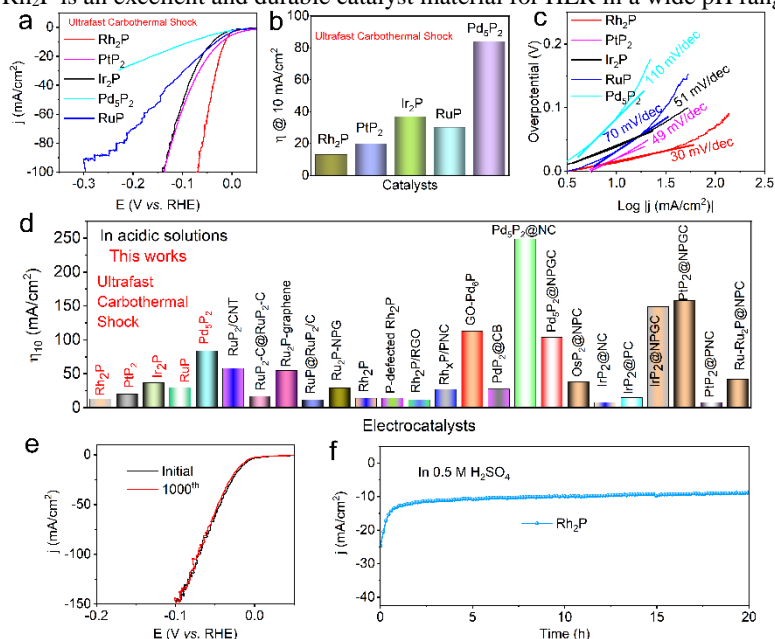


**Fig. 4.** (a, c) Polarization curves and corresponding Tafel plots of Rh<sub>2</sub>P, PtP<sub>2</sub>, Ir<sub>2</sub>P, RuP and Pd<sub>5</sub>P<sub>2</sub> in 0.5 mol/L H<sub>2</sub>SO<sub>4</sub> solution. (b) Overpotentials at  $j = 10 \text{ mA/cm}^2$  for Rh<sub>2</sub>P, PtP<sub>2</sub>, Ir<sub>2</sub>P, RuP and Pd<sub>5</sub>P<sub>2</sub>. (d) Overpotentials comparison for Rh<sub>2</sub>P, PtP<sub>2</sub>, Ir<sub>2</sub>P, RuP and Pd<sub>5</sub>P<sub>2</sub> at  $j = 10 \text{ mA/cm}^2$  with recently reported metal phosphides catalysts. (e) Polarization curves were recorded before and after 1000 CV potential cycles for Rh<sub>2</sub>P. (f) Chronoamperometric test for Rh<sub>2</sub>P in 0.5 mol/L H<sub>2</sub>SO<sub>4</sub> electrolyte at constant potential for 20 h (without  $iR$  correction).

In conclusion, we have developed a facile, energy efficient, and ultrafast carbothermal shock method capable of synthesizing TMPs within 15 s under ambient air conditions. The versatility of this technique was validated through the successful synthesis of various TMPs, including Rh<sub>2</sub>P, PtP<sub>2</sub>, Ir<sub>2</sub>P, Pd<sub>5</sub>P<sub>2</sub>, RuP and PtP<sub>2</sub>. Electrochemical measurements confirmed that all samples exhibited high HER catalytic activity, with overpotential of 13, 20, 37, 30 and 84 mV for Rh<sub>2</sub>P, PtP<sub>2</sub>, Ir<sub>2</sub>P, RuP and Pd<sub>5</sub>P<sub>2</sub> required to achieve cathodic current densities of 10 mA/cm<sup>2</sup>. This outstanding HER activity rivals that of state-of-the-art phosphides based on Pt-group metals, which are typically synthesized through conventional solid-state or solution-phase methods. Consequently, the ultrafast carbothermal shock synthesis of TMPs under ambient air conditions shows significant potential for advancing the development of TMP-based electrocatalysts for energy-related applications.

#### Acknowledgments

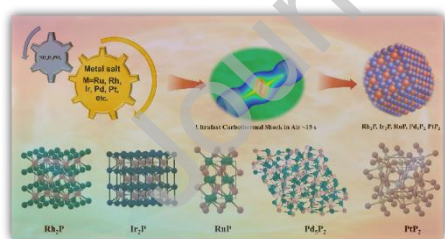
This work was supported by the National Natural Science Foundation of China (Nos. 22402030; 62475266), the Fujian Province Young and Middle-Aged Teacher Education Research Project (No. JZ240012), Youth Innovation Promotion Association of Chinese Academy of Sciences (No. 2023341) and Jiangxi Provincial Natural Science Foundation (No. 20232BAB204101).

#### References

- [1] H. D. Graven, P. Natl. Acad. Sci. U. S. A. 112 (2015) 9542-9545.
- [2] R. S. Haszeldine, Science 325 (2009) 1647.
- [3] R. D. L. Smith, M. S. Prévôt, R. D. Fagan, et al., Science 340 (2013) 60.
- [4] T. Liu, C. Chen, Z. Pu, et al., Small 20 (2024) 2405399.
- [5] H. Wei, D. Cui, J. Ma, et al., J. Mater. Chem. A 5 (2017) 1873-1894.
- [6] Z. Lu, L. Zhao, H. Fu, et al., Nat Commun. 15 (2024) 6513.
- [7] D. Xu, P. Wu, H. Tan, Inf. Funct. Mater. 1 (2024) 2-25.
- [8] Y. Gu, N. Nie, J. Liu, et al., EcoEnergy 1 (2023) 405-413.
- [9] J. Liang, Z. Cai, Z. Li, et al., Nat. Commun. 15 (2024) 2950.
- [10] J. Liang, Z. Cai, X. He, et al., Chem 10 (2024) 3067-3087.
- [11] Z. Lv, S. Zhou, L. Zhao, et al., Adv. Energy Mater. 13 (2023) 2300946.
- [12] Y. Yu, Z. Lv, Z. Liu, et al., Angew. Chem. Int. Ed. 63 (2024) e202402236.
- [13] Y. Yu, Y. Sun, J. Han, et al., Energy Environ. Sci. 17 (2024) 5183-5190.
- [14] M. Li, X. Wang, J. Meng, et al., Adv. Mater. 36 (2024) 2308628.
- [15] Z. Pu, G. Zhang, A. Hassanpour, et al., Appl. Energy 283 (2021) 116376.
- [16] Y. Zeng, C. Li, B. Li, et al., Nat. Catal. 6 (2023) 1215-1227.
- [17] P. Mardle, B. Chen, S. Holdcroft, ACS Energy Lett. 8 (2023) 3330-3342.
- [18] L. Zhao, Z. Lv, Y. Shi, et al., Energy Environ. Sci. 17 (2024) 770-779.
- [19] D. Wu, H. Du, Z. Liu, et al., EcoEnergy 2 (2024) 724-735.
- [20] W. Yu, Y. Zhang, Y. Qin, et al., Adv. Energy Mater. 13 (2023) 2203136.

- [21] Z. Pu, T. Liu, G. Zhang, et al., *Small Methods* 5 (2021) 2100699.
- [22] Z. W. Seh, J. Kibsgaard, C. F. Dickens, et al., *Science* 355 (2017) 6321.
- [23] T. Liu, C. Chen, S. Liu, et al., *Coord. Chem. Rev.* 521 (2024) 216145.
- [24] Z. Pu, T. Liu, I. S. Amiinu, et al., *Adv. Funct. Mater.* 30 (2020) 2004009.
- [25] M. Du, D. Li, S. Liu, J. Yan, *Chin. Chem. Lett.* 34 (2023) 108156.
- [26] Y. Shi, M. Li, Y. Yu, B. Zhang, *Energy Environ. Sci.* 13 (2020) 4564–4582.
- [27] C. Li, D. Zhu, S. Cheng, et al., *Chin. Chem. Lett.* 33 (2022) 1141–1153.
- [28] L. Yue, J. Liang, Z. Wu, et al., *J. Mater. Chem. A* 9 (2021) 11879–11907.
- [29] C. Tang, R. Zhang, W. Lu, et al., *Adv. Mater.* 29 (2017) 1602441.
- [30] Q. Liu, J. Tian, W. Cui, et al., *Angew. Chem. Int. Ed.* 53 (2014) 6710–6714.
- [31] L. He, Z. Cai, D. Zheng, et al., *J. Mater. Chem. A* 12 (2024) 2680–2684.
- [32] J. Tian, Q. Liu, A. M. Asiri, X. Sun, *J. Am. Chem. Soc.* 136 (2014) 7587–7590.
- [33] Q. Dong, Y. Yao, S. Cheng, et al., *Nature* 605 (2022) 470–476.
- [34] C. H. Choi, J. Shin, L. Eddy, et al., *Nat. Chem.* 16 (2024) 1831.
- [35] T. Liu, Z. Chen, S. Liu, et al., *Angew. Chem. Int. Ed.* 64 (2025) e202414021.
- [36] Z. Zhao, J. Sun, X. Li, et al., *Nat. Commun.* 15 (2024) 7475.
- [37] Z. Pu, J. Zhao, I. S. Amiinu, et al., *Energy Environ. Sci.* 12 (2019) 952–957.
- [38] B. Guo, J. Zhao, Y. Xu, et al., *ACS Appl. Mater. Interfaces* 16 (2024) 8939–8948.
- [39] Y. Liu, L. Wang, H. Zhang, et al., *Angew. Chem. Int. Ed.* 133 (2021) 22943–22950.
- [40] K. Zhou, W. Zhou, L. Yang, et al., *Adv. Funct. Mater.* 25, (2015) 7530–7538.
- [41] F. Yang, Y. Zhao, Y. Du, et al., *Adv. Energy Mater.* 8 (2018) 1703489.
- [42] Q. Qin, H. Jang, L. Chen, et al., *ACS Appl. Mater. Interfaces* 11 (2019), 16461–16473.
- [43] Y. Hong, S. Jeong, J. H. Seol, et al., *Adv. Energy Mater.* 14 (2024) 2401426.
- [44] Z. Pu, I. S. Amiinu, Z. Kou, W. Li, S. Mu, *Angew. Chem. Int. Ed.* 56 (2017) 11559–11564.
- [45] J. Yu, X. Wu, H. Zhang, et al., *ACS Appl. Energy Mater.* 2 (2019) 2645–2653.
- [46] G. Zhao, K. Rui, S. X. Dou, W. Sun, *Adv. Funct. Mater.* 28 (2018) 1803291.
- [47] M. A. Habib, S. Burse, S. Lin, et al., *Small* 20 (2024) 2307533.
- [48] C. Andronesco, S. Barwe, E. Ventosa, et al., *Angew. Chem. Int. Ed.* 56 (2017) 11258–11262.

## Graphical Abstract



Metal phosphides can be synthesized using the ultrafast carbothermal shock technique within 15 s in air.

## Declaration of Interest Statement

The authors declare that they have no known competing financial interests or personal relationships that could have appeared to influence the work reported in this paper.